Pharm Res (2014) 31:1254–1263
DOI 10.1007/s11095-013-1246-6

RESEARCH PAPER

Photo-Inducible Crosslinked Nanoassemblies for pH-Controlled Drug Release

Matthew Dickerson • Nickolas Winquist • Younsoo Bae

Received: 26 August 2013 / Accepted: 20 October 2013 / Published online: 20 November 2013

ABSTRACT

Purpose To control drug release from block copolymer nanoassemblies by variation in the degree of photo-crosslinking and inclusion of acid sensitive linkers.

Methods Poly(ethylene glycol)-poly(aspartate-hydrazide-cinnamate) (PEG-CNM) block copolymers were prepared and conjugated with a model drug, doxorubicin (DOX), through acid sensitive hydrazone linkers. The block copolymers formed photo-inducible, self-assembled nanoassemblies (piSNAs), which were used to produce photo-inducible crosslinked nanoassemblies (piCNAs) through UV crosslinking. The nanoassemblies were characterized to determine particle size, surface charge, pH- and crosslinking-dependent DOX release, *in vitro* cytotoxicity, and intracellular uptake as a function of photo-crosslinking degree.

Results Nanoassemblies with varying photo-crosslinking degrees were successfully prepared while retaining particle size and surface charge. Photo-crosslinking caused no noticeable change in DOX release from the nanoassemblies at pH 7.4, but the DOX-loaded nanoassemblies modulated drug release as a function of crosslinking at pH 6.0. The nanoassemblies showed similar cytotoxicity regardless of crosslinking degrees, presumably due to the low cellular uptake and cell nucleus drug accumulation.

Conclusions Photo-crosslinking is useful to control drug release from pH-sensitive block copolymer nanoassemblies as a function of crosslinking without altering the particle properties, and thus providing unique tools to investigate the pharmaceutical effects of drug release on cellular response.

KEY WORDS crosslinked nanoassemblies · drug carriers · drug delivery · nanoparticles · polymer micelles

M. Dickerson · N. Winquist · Y. Bae (✉)
Department of Pharmaceutical Sciences, College of Pharmacy
University of Kentucky, 789 South Limestone
Lexington, Kentucky 40536-0596, USA
e-mail: younsoo.bae@uky.edu

INTRODUCTION

Small molecule chemotherapeutics are widely employed for the treatment of many types of cancer (1–4). Chemotherapeutics are highly effective *in vitro*, but their applications *in vivo* often suffer from issues such as poor control of spatial distribution and activity over time (5,6). In addition to these factors, solubility and chemical stability in complex biological environments limit the clinical translation and application of many promising anticancer chemotherapeutics (7–9). The application of nanoparticle drug carriers with a diameter less than 100 nm has been proposed as a solution to these issues (10–12). Nanoparticles are known to preferentially accumulate in tumor tissue, which allows for the passive targeting of chemotherapeutics (13,14), while surface modification of the nanoparticles with biocompatible moieties can significantly increase circulation time in the bloodstream (15,16). Unfortunately, the physiochemical properties of nanoparticle drug carriers can change as a result of drug entrapment or release (17–21). Such critical drug carrier properties include particle size, shape, stability, and biocompatibility (22–24). Changes in these properties can result in inconsistent drug delivery leading to variable therapeutic efficacy (25–28). Consequently, there are growing needs for stable and versatile nanoparticle drug carriers that can be prepared reliably and reproducibly for efficient drug entrapment, preferential tumor delivery, and controlled release (29,30). Development of such drug carriers is also essential to ultimately controlling the spatial and temporal distribution of small molecule chemotherapeutics for the treatment of cancer as well as other human diseases, and to study the pharmaceutical effects of drug carrier modification on cellular response.

As a promising solution to prepare stable and versatile drug carriers without altering the particle properties, many crosslinked nanoparticles have been developed as drug delivery tools with improved stability and chemical versatility (31–41). However, the synthesis of crosslinked nanoparticles

often requires a lengthy optimization process to fine-tune nanoparticle synthesis and extensive purification to remove byproducts such as organic solvents or crosslinking agents (42). The physiochemical properties of many crosslinked nanoparticles are also designed to respond to environmental stimuli in order to control drug release (degradation, size change, permeability), yet changes in nanoparticle physiochemical properties make it difficult to estimate pharmacological parameters, biodistribution, antitumor activity, and toxicity. We speculated that the combined use of photo-crosslinking and degradable linker chemistry might solve these issues. Photo-crosslinking will produce stable drug carriers with fixed physiochemical properties allowing for a more accurate estimation of pharmacological properties of a drug-nanoparticle system. Moreover, it is postulated that an increase in degree of photo-cross-linking will hinder drug transport inside the nanoassembly system leading to slower release. Therefore, the central hypothesis tested in this study was that the drug release from light- and pH-sensitive block copolymer crosslinked nanoparticles can be controlled as a function of the degree of photo-crosslinking.

To test this hypothesis, we prepared a new type of drug carrier using photo-inducible crosslinked nanoassemblies (piCNAs) entrapping a model anticancer drug, doxorubicin (DOX), as illustrated in Fig. 1. A photo-crosslinking reaction takes place between light sensitive cinnamate pendant groups on poly(ethylene glycol)-poly(aspartate) block copolymers (Fig. 1b) through molecular rearrangement in response to light (43,44). In addition, these block copolymers have hydrazide drug-binding linkers for acid-labile hydrazone conjugation with DOX (45,46). Therefore, the proposed piCNA drug carriers were designed to generate no toxic byproducts, because only light is required for crosslinking, and to promote drug release in acidic tumor environments (pH < 7) while maintaining particle size (i.e. < 100 nm in diameter). The drug-loaded nanoassemblies were subsequently characterized in an *in vitro* cell culture system to determine their cytotoxicity and intracellular uptake profiles.

Taken together, this study will provide insights into controlled drug release through adjustment in the degree of photo-inducible crosslinking, which will potentially lead to developing light-programmed drug delivery systems for improving anti-cancer chemotherapy.

MATERIALS AND METHODS

Materials

The following chemicals were purchased from Sigma-Aldrich (USA): β-benzyl L-aspartate, doxorubicin hydrochloride (DOX), anhydrous hydrazine, triphosgene, anhydrous tetrahydrofuran (THF), anhydrous hexane, anhydrous N,N'-dimethylformamide (DMF), anhydrous dichloromethane (DCM), anhydrous dimethyl sulfoxide (DMSO), benzene, pyridine, and cinnamoyl chloride. Diethyl ether, phosphate buffered saline (PBS), buffer solutions (pH 6.0 and 7.4), and other chemicals were purchased from Fisher Scientific (USA). α-Methoxy-ω-amino poly(ethylene glycol) (PEG, MW = 5, 000) was purchased from NOF (Japan). 4-(2-Hydroxyethyl)-1-piperazine ethane sulfonic acid (HEPES) was purchased from Boston BioProducts (USA). Puradisc^{TM} PES syringe filters (0.2 μm) were purchased from GE Healthcare (UK). Spectra/por dialysis tubing, 50 kDa molecular cut-off (MWCO), was purchased from Spectrum Labs (USA). Slide-

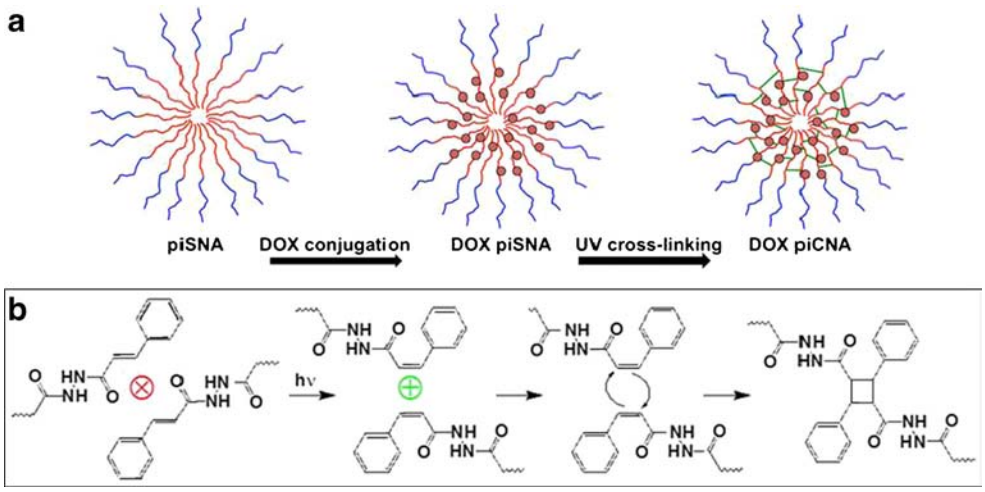

Fig. 1 Preparation of photo-inducible crosslinked nanoassemblies (piCNAs). (**a**) PEG-CNM block copolymers self-assembled to form piSNAs. DOX was chemically conjugated to the CNM block through the formation of acid sensitive hydrazone linkers. piCNAs were prepared by exposing DOX piSNAs to UV light for a predetermined time (12 or 120 min). (**b**) The mechanism of photo-crosslinking between cinnamoyl groups. UV light initiated [2 + 2] cycloaddition of adjacent cinnamate alkenes. UV exposure initiates E/Z photoisomerization crosslinking.

A-Lyzer dialysis cassettes (10 kDa MWCO, G2) were purchased from Thermo Scientific (USA). Dimethyl-d6 sulfoxide (DMSO-d6) was purchased from Cambridge Isotope Labs (USA).

Block Copolymer Synthesis

β-Benzyl-L-aspartate N-carboxy anhydride (BLA-NCA) was prepared using the Fuchs-Farthing method of synthesis as previously described (45). Briefly, BLA-NCA was prepared by reacting β-benzyl L-aspartate with triphosgene in anhydrous THF. The reaction was carried out under a nitrogen atmosphere at 45°C until the solution became clear. BLA-NCA was recrystallized from hexane at -20°C. Block copolymers were then synthesized following the procedure shown in Fig. 2. PEG-poly(β-Benzyl-L-aspartate) (PEG-BLA) was prepared as previously described (34). PEG and BLA-NCA were dissolved separately in anhydrous DMSO (100 mg/mL) under nitrogen, and then BLA-NCA was transferred to PEG and reacted at 45°C for 72 h under N_2. PEG-BLA was precipitated from solution three times using diethyl ether and lyophilized. Synthesis confirmed by proton nuclear magnetic resonance (^{1}H-NMR).

PEG-poly(aspartate-hydrazide) (PEG-HYD) block copolymers were prepared following the method reported previously (47). PEG-BLA was dissolved in benzene and dried under vacuum. PEG-BLA was then dissolved in anhydrous DMF (100 mg/mL) and reacted with distilled hydrazine (20:1 molar ratio of hydrazine to BLA). The reaction was carried out under nitrogen at 40°C for 1 h. PEG-HYD was precipitated from solution three times using diethyl ether and lyophilized. The synthesis was confirmed by ^{1}H-NMR.

Light-sensitive PEG-poly(aspartate-hydrazide-cinnamate) (PEG-CNM) block copolymers were synthesized by side chain modification. PEG-HYD (1.07 g, 0.112 mmol) was dissolved in a mixture of DCM (30 mL) and DMSO (6 mL). Pyridine (600 μL, 7.839 mmol) was added and stirred at room temperature for 10 min. Cinnamoyl chloride (650 mg, 3.920 mmol) was added and stirred overnight at room temperature under nitrogen protected from light. PEG-CNM was precipitated from solution three times using diethyl ether. PEG-CNM was dissolved in deionized water, purified through 0.2 μm Puradisc^{TM} PES syringe filters, and dialyzed using 50 kDa MWCO spectra/por dialysis tubing. Purified PEG-CNM was lyophilized. Cinnamate conjugation was confirmed by ^{1}H-NMR analysis in DMSO-d6 and by UV/visible (UV/Vis) spectroscopy.

The Synthesis of Photo-Inducible Crosslinked Nanoassembly (piCNA)

Photo-inducible self-assembled nanoassemblies (0.5 mg/mL) (piSNAs) were prepared from PEG-CNM in deionized water. The aqueous solution containing piSNAs was incubated under a UV Lamp (model UVGL-55, 1,600 μW/cm^2, UVP, USA) for 0, 30, 60, 120, or 1,440 min to form photo-inducible crosslinked nanoassemblies (piCNAs). The crosslinking reaction was monitored by measuring the change in polymer absorbance at 285 nm as a function of light exposure time. Measurements were carried out using a Spectramax M5 plate reader equipped with SoftMax Pro software (Molecular Devices, USA). The effects of crosslinking on piCNA particle size and surface charge were determined in 1x phosphate buffered saline (PBS) using a Zetasizer Nano ZS (Malvern, USA) while molecular weight was estimated based on a PEG standard curve using gel permeation chromatography (GPC) with a superose 12 10/300 GL column and 1x PBS as a running buffer.

Drug Entrapment and Release

DOX was chemically conjugated to PEG-CNM through pH sensitive hydrazone bonds to form PEG-CNM-DOX,

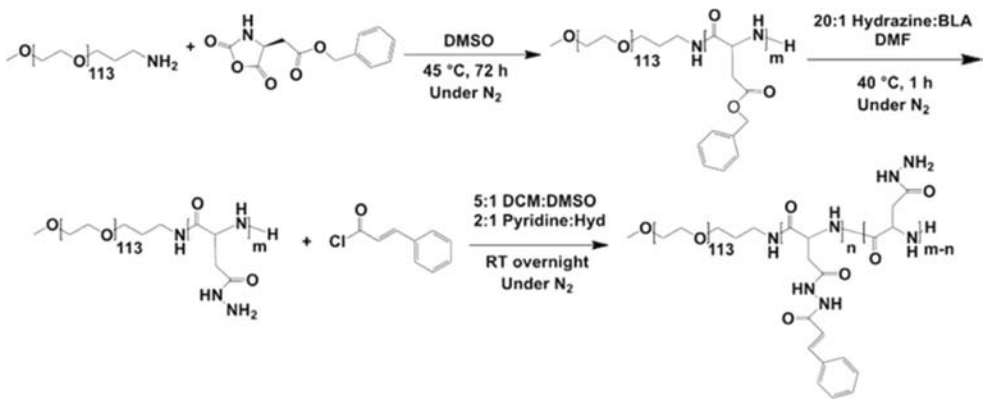

Fig. 2 Synthesis scheme of light-sensitive block copolymers. PEG was reacted with BLA-NCA in anhydrous DMSO at 45°C for 72 h to generate PEG-BLA, which was converted to PEG-HYD using a 20:1 ratio of anhydrous hydrazine to BLA groups in anhydrous DMF. Cinnamate pendant groups were added by incubating PEG-HYD and cinnamoyl chloride at room temperature overnight in a 5:1 mixture of anhydrous DCM and anhydrous DMSO with a 2:1 ratio of pyridine to HYD groups.

following the method that we previously reported (45). Conjugation in this manner slows DOX release at physiological pH compared to the intracellular endosomal pH 6.0 (48,49). PEG-CNM (100 mg) and DOX (50 mg) were dissolved in DMSO (5 mL) and incubated at room temperature with gentle agitation for 6 days protected from light. PEG-CNM polymer was conjugated with DOX prior to crosslinking to ensure maximum loading efficiency. PEG-CNM-DOX was collected by precipitating in diethyl ether three times. Physically bound DOX was removed from PEG-CNM by using a Sephadex LH-20 column (GE Healthcare) with a methanol mobile phase. This ensured that only chemically conjugated DOX remained. Solvent was removed from PEG-CNM-DOX under reduced pressure, and the PEG-CNM-DOX was freeze-dried.

The effect of the degree of photo-crosslinking on DOX release rate was determined for PEG-CNM-DOX piSNAs (DOX piSNAs), PEG-CNM-DOX piCNAs that were crosslinked for 12 min (DOX 12-piCNAs), and PEG-CNM-DOX piCNAs that were crosslinked for 120 min (DOX 12-piCNAs). DOX piSNAs (1 mg/mL) were prepared in deionized water and crosslinked under the conditions above to generate DOX 12-piCNAs and DOX 120-piCNAs. Samples (0.5 mL, $n=3$) were dialyzed in 10 kDa MWCO G2 Slide-A-Lyzer dialysis cassettes in 5 L of buffer at pH 6.0 (10 mM phosphate buffer) or pH 7.4 (10 mM HEPES). Samples (20 μL) were taken from the dialysis cassettes at 0, 30, 60, 180, 360, and 1,440 min. All samples were diluted with 80 μL of DMSO, and DOX concentration was determined by UV/Vis spectroscopy. The mass of DOX remaining was determined based on a calibration curve prepared using free DOX in 80% DMSO and 20% deionized water. DOX release kinetics and the area under the concentration curve (AUC) were analyzed based on two-phase decay, nonlinear regression in Prism 5 from GraphPad Software.

Cytotoxicity Evaluation

The cytotoxicity of DOX piSNAs, DOX 12-piCNAs, and DOX 120-piCNAs was evaluated in comparison to free DOX in human lung cancer A549 cells from the American Type Culture Collection (ATCC). A549 cells were cultured as per supplier instructions at 37°C, 5% CO_2. Cells were seeded in 96-well plates (5,000 cells/well) and incubated at 37°C, 5% CO_2. After 24 h, 100 μL of samples at varying concentrations were added to the wells ($n=8$). The cells were incubated for 72 h at 37°C, 5% CO_2. Cell viability was then determined using a resazurin assay, which measures mitochondrial metabolic activity in living cells. Cell viability was determined after 3 h by measuring fluorescence with emission (Em) at 590 nm and excitation (Ex) at 560 nm. Sample cytotoxicity was compared with respect to the median inhibitory concentration (IC_{50}) of free drug.

Cell Internalization Observation

The cell internalization of DOX piSNAs, DOX 12-piCNAs, and DOX 120-piCNAs was evaluated in A549 human lung cancer cells in comparison to free DOX. A549 cells were seeded in 8-well Millicell EZ slides from Millipore (USA) at a density of 8,000 cells/well and incubated overnight at 37°C, 5% CO_2. A549 cells were then incubated with 100 mM of DOX piSNAs, DOX 12-piCNAs, and DOX 120-piCNAs, or free DOX for 1, 6, 24, or 48 h. After each time interval, sample solutions were removed, cells were washed 3 times with 1x PBS, and nuclei were stained with Hoechst 33342 (1 μL / 2 mL 1x PBS) for microscopic observations. DOX was visualized using a Nikon Eclipse LV 100 fluorescent microscope at 20× magnification with a Ds RED HC HiSN Zero Shift Filter set (Ex: 530 – 560 nm, Em: 590 – 650 nm) while stained nuclei were visualized using a DAPI HC HiSN Zero Shift Filter set (Ex: 325 – 375 nm, Em: 435 – 485 nm). All images were processed using NIS-Elements BR 3.0 software.

Statistical Analysis

Data is described as mean and standard deviation unless otherwise indicated. The one-way analysis of variance (ANOVA) test was conducted on A549 cell cytotoxicity results to determine statistically significant differences ($p=0.05$), using Prism 5 from GraphPad Software (USA).

RESULTS AND DISCUSSION

Block Copolymer Synthesis

^{1}H-NMR confirmed successful modification of the poly(aspartate-hydrazide) with cinnamate groups. The peaks located between 8.0 and 9.2 ppm for PEG-Hyd in Fig. 3a are indicative of side-chain hydrazide functionalization while the large peak from 3.6 to 3.8 ppm coincides with PEG. When reacted with cinnamoyl chloride the peaks between 8.0 and 9.2 ppm peaks disappeared and were replaced by the doublet in Fig. 3b from 7.3 to 7.6 ppm that corresponds to the 5 aromatic hydrogens on the benzene ring of cinnamate. In comparison to Fig. 3a, the peaks from a polymer backbone in Fig. 3b decreased substantially. Only the peaks from PEG and cinnamate rings showed sufficient NMR signal intensity and resolution for quantification. These results suggest that PEG and cinnamate groups have greater molecular mobility than the polymer backbone. Therefore, the number of cinnamate side chain additions per PEG-CNM was estimated by comparing the area of the cinnamate peaks (50.1 protons) to the area of the 5 k PEG peak (455.0 protons per chain). The peak area comparison showed that 29% of available binding

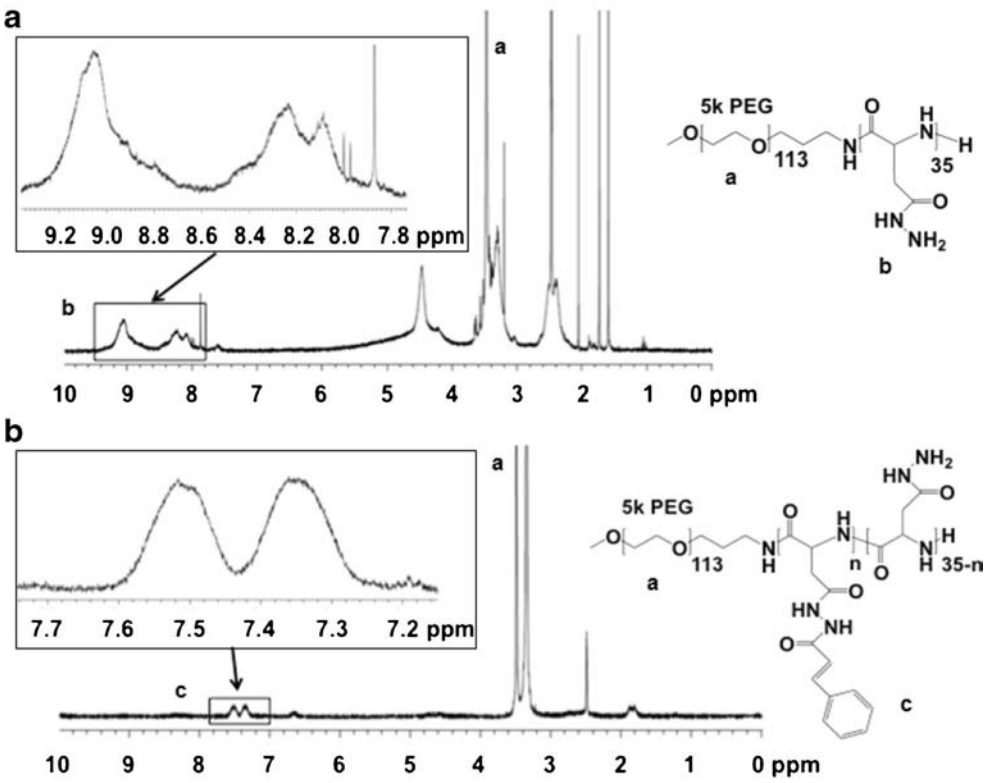

Fig. 3 ^{1}H-NMR spectra for PEG-Hyd (**a**) and PEG-CNM (**b**) block copolymers. Successful reactions were confirmed by peak validation of protecting or pendant groups.

sites were functionalized with cinnamate groups for an average of 10 cinnamate groups per polymer chain.

Synthesis and Characterization of piCNA

The absorbance of PEG-CNM at 285 nm was tracked as a function of UV exposure time to monitor the extent of polymer crosslinking (Fig. 4). The change in absorbance spectra is illustrated in Fig. 4a while the degree of potential crosslinking is shown in Fig. 4b. The majority of crosslinking took place within 2 h as the degree of crosslinking increased very little between 2 and 24 h. The molecular weight, particle diameter, and surface charges of piSNAs and piCNAs photo-crosslinked between 30 and 120 min were obtained using GPC and light scattering techniques. GPC results for piSNAs and piCNAs photo-crosslinked for 120 min are shown in Fig. 5. Sample molecular weights were estimated based on the elution of PEG standards of known molecular weights. The molecular weight of piSNAs was 387 kDa and did not change after 120 min of photo-crosslinking. Table I summarizes the particle size and surface charges of piSNAs and piCNAs. All groups had a sub-100 nm hydrodynamic diameter of approximately 30 nm and neutral surface charge ($\zeta = +/- 10$ mV). These results demonstrate that PEG-CNMs self-assembled to form micelles and subsequent photo-crosslinking does not significantly alter the physical properties of the nanoassemblies.

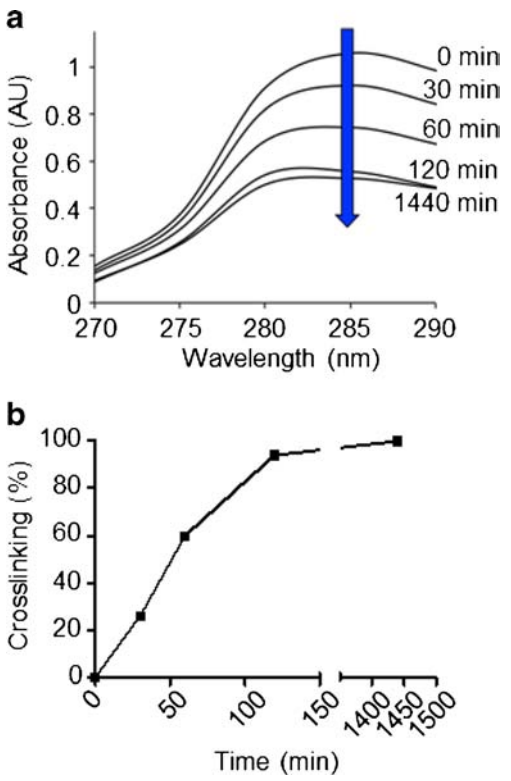

Fig. 4 Time-dependent monitoring of photo-crosslinking reaction. PEG-CNM photo-crosslinking was confirmed. (**a**) Core crosslinking between cinnamate groups monitored by absorbance change at 285 nm. (**b**) Degree of potential crosslinking as a function of UV exposure time.

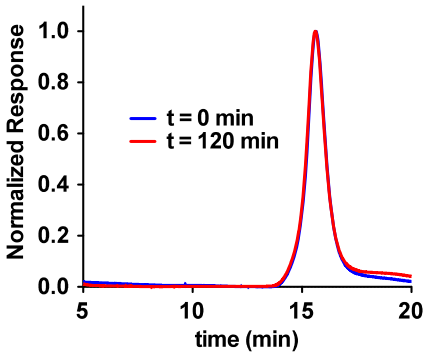

Fig. 5 GPC analysis of piSNAs and 120-piCNAs. The molecular weight of 120-piCNAs was indistinguishable from piSNAs.

As the application of nanoscale materials for anti-cancer drug delivery continues to evolve, one of the main issues confronting the field is to control the spatial and temporal distribution of therapeutic payloads in the body. The challenge is to develop drug carriers that remain stable while circulating in the bloodstream and efficiently release their drug cargo once they accumulate in a disease site such as solid tumors. Formation of stable bonds between polymer subunits shown in Fig. 1 was intended to generate nanoassembly drug carriers with improved long-term stability *in vivo*. By modulating crosslinking yield by controlling UV exposure time it would be also possible to tune the release rate of entrapped therapeutics.

The UV/Vis spectrum of piSNAs suspended in deionized water confirmed cinnamate photo-crosslinking that proceeded as a function of UV exposure time. But it is also possible that cinnamates might simply undergo reversible isomerization in addition to photodimerization of adjacent cinnamates resulting in crosslinking (43). A clear isosbestic point in the UV/Vis spectrum can be observed when reversible isomerization is taking place. The absence of clear isosbestic points in Fig. 4a indicates that cinnamate photodimerization through [2+2] cycloaddition between the double bonds of two adjacent cinnamates (illustrated in Fig. 2) dominated cinnamate E/Z photoisomerization leading to the formation of core crosslinked piCNAs (43). In the meantime, the size, surface charge, and molecular weight of piCNAs were indistinguishable from piSNAs (Fig. 5). This suggests that the physiochemical properties of piCNAs remained unaltered compared to piSNAs after photo-crosslinking. piCNAs with sub-100 nm diameters and a neutral surface charge were synthesized, which were suitable for further *in vitro* testing.

Table I Physiochemical Characterization of piCNAs

Crosslinking Time (min)	Diameter (nm)	Zeta-potential (mV)
0	26.2 ± 4.0	7.3 ± 0.1
30	31.5 ± 8.9	6.7 ± 0.6
60	25.1 ± 5.1	8.3 ± 0.4
120	27.1 ± 3.3	7.4 ± 0.5

Drug Entrapment and Release Profiles

Release of a model drug (DOX) was compared for the nanoassemblies with variable degrees of crosslinking to determine if drug release rate would be controlled by varying UV exposure time. Based on Fig. 4b, UV exposure times were selected that corresponded with 10% (12 min) and 100% (120 min) piCNA photo-crosslinking. DOX release from piCNA formulations was compared to release from piSNAs. DOX loading in piSNAs was 27.6 ± 0.6 wt%, in 12-piCNAs it was 26.4 ± 1.4 wt%, and in 120-piCNAs it was 25.7 ± 1.9 wt% (Table II). Release profiles of DOX from piSNAs, 12-piCNAs, and 120-piCNAs are shown in Fig. 6 while rate constants and AUC values are shown in Table II. At pH 7.4 (Fig. 6a), DOX release was slower (60% initial payload remaining after 24 h) and independent of crosslinking. As shown in Fig. 6b, DOX release increased at pH 6.0 (31% initial payload remaining after 24 h for piSNAs and 12-piCNAs, and 48% initial payload remaining after 24 h for 120-piCNAs). DOX release was best represented with two-phase nonlinear decay composed of a fast phase defined by (K_{fast}) and a slow phase defined by (K_{slow}). At pH 7.4, K_{fast} and K_{slow} for DOX release were similar for piSNAs, 12-piCNAs, and 120-piCNAs. At pH 6.0, corresponding to the intracellular endosomal pH, DOX release from 120-piCNAs was significantly slower than DOX release from piSNAs or 12-piCNAs ($p < 0.05$) primarily due to a smaller K_{fast} (0.6 ± 0.4) and a lower% fast phase (24%) compared to piSNAs (K_{fast} = 1.5 ± 0.2 and% fast phase = 56.7%) or 12-piCNAs (K_{fast} = 1.6 ± 0.3 and% fast phase = 48.2%). Similarly, the% fast phase was shorter at pH 7.4 (31.4 – 39.2%) than at pH 6.0 except for 120-piCNAs. In all cases, K_{slow} values were indistinguishable. Results indicated that photo-crosslinking of piSNAs did not affect DOX release rate at pH 7.4, but DOX release at pH 6.0 slowed down as the degree of photo-crosslinking increased.

DOX release at pH 7.4 and 6.0 was biphasic, characterized by initial rapid release followed by a slower secondary release. The observed change in release kinetics may be attributed to non-covalent interactions between DOX and drug carriers. Increased DOX release rate at pH 6.0 was due to the presence of acid cleavable hydrazone drug linkers. The degree of crosslinking affected the release rate of DOX at pH 6.0 but not at pH 7.4. This may be due to the rate of hydrazone bond cleavage compared to DOX release. At pH 7.4 the hydrazone bonds between DOX and the carriers were relatively stable and likely rate limiting for drug release. As a result, DOX release from piSNAs, 12-

Table II Kinetic Analysis of DOX Release from piSNAs and piCNAs

Crosslinking time (min)	DOX loading (wt%)	pH	K_{fast}	K_{slow}	% Fast	AUC
0	27.6 ± 0.6	6.0	1.5 ± 0.2	0.03 ± 0.01	56.7	2,866
		7.4	0.7 ± 0.4	0.02 ± 0.01	39.2	7,986
12	26.4 ± 1.4	6.0	1.6 ± 0.3	0.04 ± 0.01	48.2	3,032
		7.4	2.0 ± 0.6	0.03 ± 0.01	35.9	7,346
120	25.7 ± 1.9	6.0	0.6 ± 0.4	0.04 ± 0.01	24.0	4,256
		7.4	0.9 ± 0.3	0.03 ± 0.01	31.4	7,681

piCNAs, and 120-piCNAs was indistinguishable. However, at pH 6.0 the acid sensitive hydrazone bonds degraded more quickly. The rate of release from 120-piCNAs (100% potential crosslinking) was slowed significantly compared to 12-piCNAs (10% potential crosslinking) and piSNAs demonstrating the effect of the degree of crosslinking on drug release from piCNAs. This implies that particle stabilization through minimal photo-crosslinking is not be sufficient to slow DOX release but there is a threshold above which degree of crosslinking can potentially decrease the rate of drug release.

Cytotoxicity and Cell Internalization Patterns

In order to elucidate the effect of chemical conjugation of DOX to PEG-CNM and the impact of photo-crosslinking on the activity of conjugated DOX, cytotoxicity and intracellular uptake of drug-loaded nanoparticles were evaluated in A549 human lung cancer cells. A549 dose-response curves are shown in Fig. 7 after a 72 h exposure time to free DOX, DOX piSNAs, DOX 12-piCNAs, and DOX 120-piCNAs ($n = 8$). Free DOX was the most potent (0.4 ± 0.1 μM, $p < 0.05$) while the activity of DOX piSNAs (7.8 ± 4.0 μM), DOX 12-piCNAs (11.7 ± 6.3 μM), and DOX 120-piCNAs (10.9 ± 4.5 μM) were not significantly different. A549 cells internalized all formulations after 6 h with free DOX spread through the entire cell including the nucleus (Fig. 8). DOX piSNAs and DOX piCNAs were located primarily outside the nucleus even after 24 h of exposure. Comparable cytotoxicity of DOX piSNAs and piCNAs resulted from similar apparent internalization rates for the formulations followed by entrapment in endosomes. Sequestration in endosomes may have resulted from the ionization of DOX, which is a weak base. This would impede the movement of ionized DOX through endosomal membranes, into the cytosol, and subsequently into the nucleus. Thus, while DOX 120-piCNAs released DOX more slowly at pH 6.0, transfer of DOX out of endosomes limited the therapeutic effect leading to comparable cytotoxicity between the formulations. Endosomal entrapment of DOX piSNA and piCNA formulations may also account for the difference in cytotoxicity compared to free DOX as it limits accumulation in the nucleus.

Initially, some reduction in DOX activity was anticipated as a result of exposure to UV light during photo-crosslinking due to generation of radical species. However, it was previously demonstrated that Doxil (a liposomal formulation of DOX) degraded at a slower rate than free DOX in solution when exposed to UV light (50). It is believed that this was due to a shielding effect that resulted from many DOX molecules being in close proximity. After 2 h of irradiation (1.3 – 1.4 mW/cm^2) the activity of Doxil remained greater than 80% (50). Based on this, a similar protecting effect was expected for DOX piCNAs. While there was a 20 fold reduction in the potency of DOX piSNA and DOX piCNA formulations compared to free

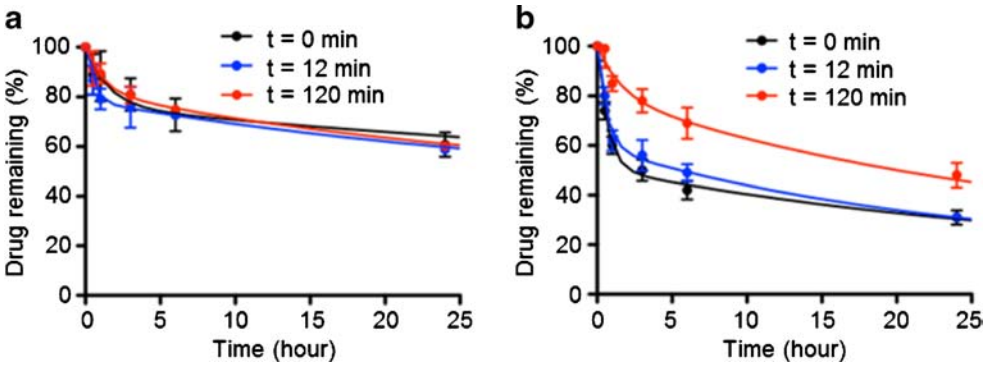

Fig. 6 DOX release from various piSNAs and piCNAs formulations at the physiological pH 7.4 (**a**) or intracellular endosomal pH 6.0 (**b**). The piSNAs and piCNAs were crosslinked with 254 nm UV light for 12 or 120 min.

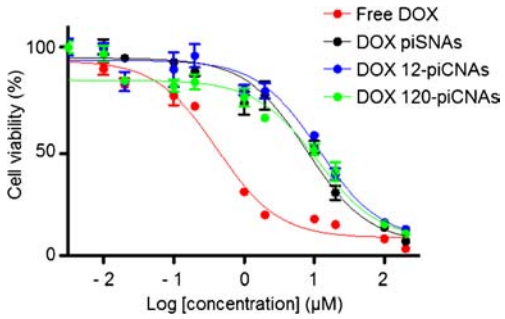

Fig. 7 Dose-response curves of piCNAs against human lung A549 cancer cells. Cell viability was determined after a sample exposure time of 72 h. The median inhibitory concentrations (IC_{50}) were: free DOX = 0.4 ± 0.1 μM, DOX piSNAs = 7.8 ± 4.0 μM, DOX 12-piCNAs = 11.7 ± 6.3 μM, and DOX 120-piCNAs = 10.9 ± 4.5 μM ($n = 8$).

DOX ($p < 0.05$), there was no statistical difference between the activity of DOX piSNAs and DOX piCNAs. This suggests that UV irradiation did not significantly reduce DOX potency and that the change observed in cell cytotoxicity was likely due to differences in intracellular localization as a result of conjugation with piSNAs or piCNAs.

Fluorescence imaging of uptake into A549 cells further supported this idea (Fig. 8). While uptake was observed for all DOX piSNA and DOX piCNA formulations after 6 h they were primarily concentrated in the cellular cytoplasm rather than the nuclei even after 24 h. This was in contrast to free DOX, which after 6 h was distributed throughout the entire cell. DNA damage through inhibition of topoisomerase II inhibition leading to cell apoptosis is a major mechanism of DOX anticancer activity (51). Thus, the apparent inability of piSNA and piCNA formulations to quickly enter the nucleus and interact with the DNA of target cells greatly reduces the cytotoxic potential. These results indicate that further study is necessary to investigate the pharmaceutical effects of pH-controlled drug release on cellular response.

CONCLUSION

Photo-inducible crosslinked nanoassemblies for pH-controlled drug release were successfully synthesized. Crosslinking did not significantly impact the physiochemical properties of the nanoassemblies at pH 7.4, yet an increase in the degree of crosslinking was confirmed to slow drug release at pH 6.0, corresponding to the intracellular endosomal environment. Cell studies revealed that DOX-conjugated nanoassemblies showed similar *in vitro* anticancer activity regardless of photo-crosslinking degrees while their cytotoxicity was always lower than free drugs, presumably due to low cellular uptake of the nanoassemblies. In conclusion, we confirmed in this study that drug release from light- and pH-sensitive block copolymer crosslinked nanoparticles can be controlled as a function of the degree of photo-crosslinking. The photo-inducible crosslinked nanoassemblies are expected to provide useful and unique tools to study the effects of controlled drug release on cellular response while maintaining the particle size, stability, and surface properties of the nanoparticle drug carriers.

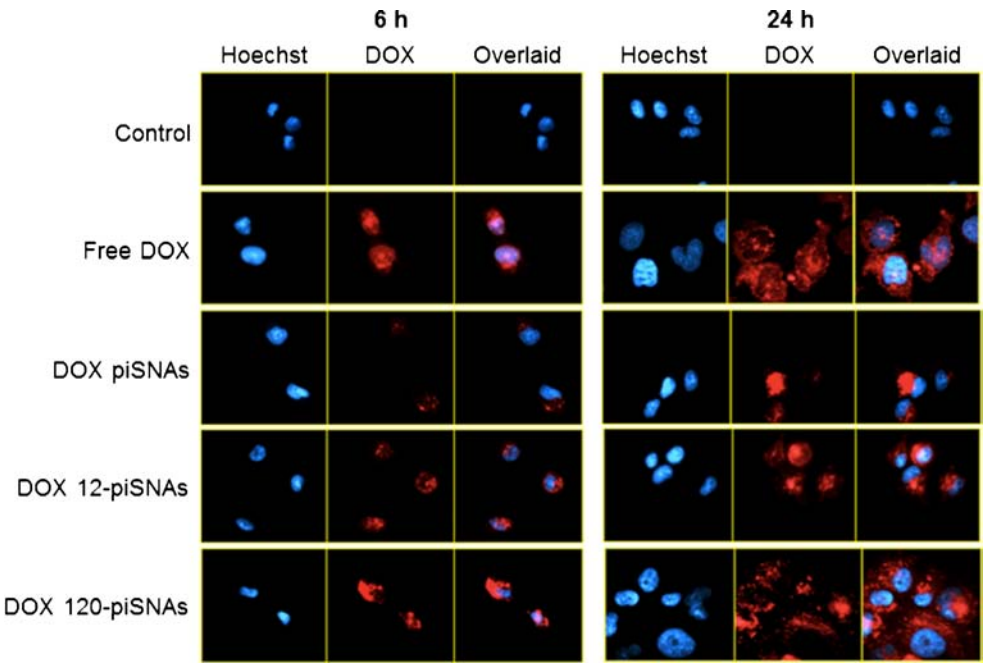

Fig. 8 Time-dependent changes in accumulation of DOX piSNAs and DOX piCNAs inside A549 cells. Representative fluorescence microscope images taken at 20 × magnification are shown for intracellular uptake of free DOX, DOX piSNAs, DOX 12-piCNAs, and DOX 120-piCNAs after an exposure time of 6 h and 24 h. Rapid internalization displayed by all sample groups. DOX piSNA and DOX piCNA formulations accumulated in the cytoplasm of cells while free DOX was located in both the nucleus and cytoplasm after 6 h. After 24 h DOX distribution was similar except that DOX from 120-piCNAs appeared more diffuse than piSNAs or 12-piCNAs.

ACKNOWLEDGMENTS AND DISCLOSURES

MD acknowledges the University of Kentucky Cancer Nanotechnology Training Center (UK-CNTC) postdoctoral traineeship, supported by the NCI/NIH and part of the National Cancer Institute Alliance for Nanotechnology in Cancer (5R25CA153954).

REFERENCES

1. Imai K, Takaoka A. Comparing antibody and small-molecule therapies for cancer. Nat Rev Cancer. 2006;6:714–27.
2. Hennessy BT, Smith DL, Ram PT, Lu Y, Mills GB. Exploiting the PI3K/AKT pathways for cancer drug discovery. Cancer Rev Drug Discov. 2005;4:988–1004.
3. Kelland L. The resurgence of platinum-based cancer chemotherapy. Nat Rev Cancer. 2007;7:573–84.
4. Johnstone RW. Histone-deacetylase inhibitors: novel drugs for the treatment of cancer. Nat Rev Drug Discov. 2002;1:287–99.
5. Kawabata-Shoda E, Masuda S, Kimura H. Anticancer drug development from traditional cytotoxic to targeted therapies: evidence of shorter drug research and development time, and shorter drug lag in Japan. J Clin Pharm Ther. 2012;37(5):547–52.
6. Atkins JH, Gershell LJ. Selective anticancer drugs. Nat Rev Drug Discov. 2002;1(7):491–2.
7. Wood AJJ. Side effects of adjuvant treatment of breast cancer. New Engl J Med. 2001;344:1997–2008.
8. Johnstone RW, Ruefli AA, Lowe SW. Apoptosis: a link between cancer genetics and chemotherapy. Cell. 2002;108:153–64.
9. Brigger I, Dubernet C, Couvreur P. Nanoparticles in cancer therapy and diagnosis. Adv Drug Deliv Rev. 2012;64:24–36.
10. Brannon-Peppas L, Blanchette JO. Nanoparticle and targeted systems for cancer therapy. Adv Drug Deliv Rev. 2012;64(Supplement):206–12.
11. Peer D, Karp JM, Hong S, Farokhazad OC, Margalit R, Langer R. Nanocarriers as an emerging platform for cancer therapy. Nat Nanotechnol. 2007;2:751–60.
12. Davis ME, Chen Z, Shin DM. Nanoparticle therapeutics: an emerging treatment modality for cancer. Nat Rev Drug Discov. 2008;7:771–82.
13. Maeda H, Matsumura Y. EPR effect based drug design and clinical outlook for enhanced cancer chemotherapy. Adv Drug Deliv Rev. 2011;63(3):129–30.
14. Maeda H. Tumor-selective delivery of macromolecular drugs via the EPR effect: background and future prospects. Bioconjug Chem. 2010;21(5):797–802.
15. Mahon E, Salvati A, Baldelli Bombelli F, Lynch I, Dawson KA. Designing the nanoparticle-biomolecule interface for "targeting and therapeutic delivery". J Control Release. 2012;161(2):164–74.
16. Petros RA, DeSimone JM. Strategies in the design of nanoparticles for therapeutic applications. Nat Rev Drug Discov. 2010;9(8):615–27.
17. Bourzac K. Nanotechnology: carrying drugs. Nature. 2012;491(7425):S58–60.
18. Yokoyama M. Polymeric micelles as a new drug carrier system and their required considerations for clinical trials. Expert Opin Drug Del. 2010;7(2):145–58.
19. Oerlemans C, Bult W, Bos M, Storm G, Nijsen JF, Hennink WE. Polymeric micelles in anticancer therapy: targeting, imaging and triggered release. Pharm Res. 2010;27(12):2569–89.
20. Vicent MJ, Ringsdorf H, Duncan R. Polymer therapeutics: clinical applications and challenges for development. Adv Drug Deliv Rev. 2009;61(13):1117–20.
21. Matsumura Y, Kataoka K. Preclinical and clinical studies of anticancer agent-incorporating polymer micelles. Cancer Sci. 2009;100(4):572–9.
22. Perrault SD, Walkey C, Jennings T, Fischer HC, Chan WCW. Mediating tumor targeting efficiency of nanoparticles through design. Nano Lett. 2009;9:1909–15.
23. Albanese A, Tang PS, Chan WCW. The effect of nanoparticle size, shape, and surface chemistry on biological systems. Annu Rev Biomed Eng. 2012;14:1–16.
24. He C, Hu Y, Yin L, Tang C, Yin C. Effects of particle size and surface charge on cellular uptake and biodistribution of polymeric nanoparticles. Biomaterials. 2010;31:3657–66.
25. Ruenraroengsak P, Cook JM, Florence AT. Nanosystem drug targeting: facing up to complex realities. J Control Release. 2010;141(3):265–76.
26. Kell DB, Dobson PD, Oliver SG. Pharmaceutical drug transport: the issues and the implications that it is essentially carrier-mediated only. Drug Discov Today. 2011;16(15–16):704–14.
27. Anraku Y, Kishimura A, Kobayashi A, Oba M, Kataoka K. Size-controlled long-circulating PICsome as a ruler to measure critical cut-off disposition size into normal and tumor tissues. Chem Commun. 2011;47(21):6054–6.
28. Stella VJ. Prodrugs: some thoughts and current issues. J Pharm Sci. 2010;99(12):4755–65.
29. Lee HJ, Bae Y. Pharmaceutical differences between block copolymer self-assembled and cross-linked nanoassemblies as carriers for tunable drug release. Pharm Res. 2013;30(2):478–88.
30. Lee HJ, Ponta A, Bae Y. Polymer nanoassemblies for cancer treatment and imaging. Ther Deliv. 2010;1(6):803–17.
31. Yallapu MM, Jaggi M, Chauhan S. Design and engineering of nanogels for cancer treatment. Drug Discov Today. 2011;16:457–63.
32. Shuai X, Merdan T, Schaper AK, Xi F, Kissel T. Core-cross-linked polymeric micelles as paclitaxel carriers. Bioconjug Chem. 2004;15:441–8.
33. Sun G, Hagooly A, Xu J, Nystrom AM, Li Z, Rossin R, *et al*. Facile, efficient approach to accomplish tunable chemistries and variable biodistributions for shell cross-linked nanoparticles. Biomacromolecules. 2008;9:1997–2006.
34. Lee HJ, Bae Y. Cross-linked nanoassemblies from poly(ethylene glycol)-poly(aspartate) block copolymers as stable supramolecular templates for particulate drug delivery. Biomacromolecules. 2011;12:2686–96.
35. Oberoi HS, Laquer FC, Marky LA, Kabanov AV, Bronich TK. Core cross-linked block ionomer micelles as pH-responsive carriers for cis-diamminedichloroplatinum(II). J Control Release. 2011;153(1):64–72.
36. Sahay G, Kim JO, Kabanov AV, Bronich TK. The exploitation of differential endocytic pathways in normal and tumor cells in the selective targeting of nanoparticulate chemotherapeutic agents. Biomaterials. 2010;31(5):923–33.
37. Kim JO, Sahay G, Kabanov AV, Bronich TK. Polymeric micelles with ionic cores containing biodegradable cross-links for delivery of chemotherapeutic agents. Biomacromolecules. 2010;11(4):919–26.
38. Bontha S, Kabanov AV, Bronich TK. Polymer micelles with cross-linked ionic cores for delivery of anticancer drugs. J Control Release. 2006;114(2):163–74.
39. Li Y, Hindi K, Watts Kristin M, Taylor Jane B, Zhang K, Li Z, *et al*. Shell crosslinked nanoparticles carrying silver antimicrobials as therapeutics. Chem Commun. 2010;46(1):121–3.
40. Van Horn BA, Wooley KL. Toward cross-linked degradable polyester materials: investigations into the compatibility and use of

reductive amination chemistry for cross-linking. Macromolecules. 2007;40(5):1480–8.
41. O'Reilly RK, Joralemon MJ, Hawker CJ, Wooley KL. Facile syntheses of surface-functionalized micelles and shell cross-linked nanoparticles. J Polym Sci Part A Polym Chem. 2006;44(17):5203–17.
42. Cheng Z, Al Zaki A, Hui JZ, Muzykantov VR, Tsourkas A. Multifunctional nanoparticles: cost versus benefit of adding targeting and imaging capabilities. Science. 2012;338(6109):903–10.
43. Ali AH, Srinivasan KSV. Synthesis, characterization, and studies on the solid-state cross-linking of functionalized vinyl cinnamate polymers. J App Polym Sci. 1997;67:441–8.
44. Sung S-J, Cho K-Y, Hah H, Lee J, Shim H-K, Park J-K. Two different reaction mechanisms of cinnamate side groups attached to the various polymer backbones. Polymer. 2006;47:2314–21.
45. Bae Y, Fukushima S, Harada A, Kataoka K. Design of environment-sensitive supramulecular assemblies for intracellular drug delivery: polymeric micelles that are responsive to intracellular pH change. Angew Chem Int Ed. 2003;42:4640–3.
46. Bae Y, Jang W-D, Nishiyama N, Fukushima S, Kataoka K. Multifunctional polymeric micelles with folate-mediated cancer cell targeting and pH-triggered drug releasing properties for active intracellular drug delivery. Mol BioSyst. 2005;1(3):242–50.
47. Scott D, Rohr J, Bae Y. Nanoparticulate formulations of mithramycin analogs for enhanced cytotoxicity. Int J Nanomed. 2011;6:2757–67.
48. West KR, Otto S. Reversible covalent chemistry in drug delivery. Curr Drug Discov Technol. 2005;2(3):123–60.
49. Jones AT, Gumbleton M, Duncan R. Understanding endocytic pathways and intracellular trafficking: a prerequisite for effective design of advanced drug delivery systems. Adv Drug Deliv Rev. 2003;55(11):1353–7.
50. Bandak S, Ramu A, Barenholz Y, Gabizon A. Reduced UV-induced degradation of doxorubicin encapsulated in polyethyleneglycol-coated liposomes. Pharm Res. 1999;6:841–6.
51. Mizutani H, Tada-Oikawa S, Hiraku Y, Kojima M, Kawanishi S. Mechanism of apoptosis induced by doxorubicin through the generation of hydrogen peroxide. Life Sci. 2005;76:1439–53.